ChemistrySelect

Research Article
doi.org/10.1002/slct.202402704

Chemistry Europe
European Chemical Societies Publishing

www.chemistryselect.org

Ligand Backbone Influenced Luminescent Properties of Mononuclear Zn(II)-N3Py2 Compounds: Synthesis, Structures and Nitroaromatics Detection

Jeffrey L. Viegas,[a, b] Vishnu R. Chari,[a] and Sunder N. Dhuri*[a]

Mononuclear Zn(II) compounds, $[Zn(L^1)](ClO_4)_2$ (**1**) and $[Zn(L^2)](ClO_4)_2$ (**2**), embedded with ligands, $L^1 = N^1$-(pyridin-2-ylmethyl)-N^2-(2-((pyridin-2-ylmethyl)amino)ethyl)ethane-1,2-diamine and $L^2 = N^1$-(pyridin-2-ylmethyl)-N^3-(3-((pyridin-2-ylmethyl)amino)propyl)propane-1,3-diamine are synthesized. Compound **1** is revisited, and structure-function relation is compared with new compound **2**. Single crystal X-ray analysis revealed that compound **1** crystallizes in the tetragonal non-centrosymmetric $P4_1$ space group while **2** crystallizes in a centrosymmetric monoclinic space group $P2_1/c$. The asymmetric unit consists of a crystallographically independent $[Zn(L^1)]^{2+}$ cation in **1** while $[Zn(L^2)]^{2+}$cation in **2** and two unique perchlorate anions in both. IR spectra of **1** and **2** confirmed the vibrations due to organic ligands and tetrahedral perchlorates. PXRD confirmed the phase purity of powdered samples compared with theoretical PXRD patterns obtained from single-crystal X-ray diffraction data. NMR and ESI-MS data suggested the phase purity and stability of compounds **1** and **2** in solution. Photoluminescence properties of compounds **1** and **2** have been investigated, considering their application in sensing explosive nitroaromatic compounds. Our results suggest that compound **1** is very selective in the chemical sensing of trinitrophenol (TNP) and dinitrophenol (DNP) in an aqueous medium compared to the reactivity of compound **2**. The existence of spectral overlap in the absorption spectra of 2,4-dinitrophenol (DNP) and 2,4,6-trinitrophenol (TNP) with the emission spectrum of **1** or **2** indicates the operation of the resonance electron transfer (RET) mechanism.

1. Introduction

Sustainable development has significantly stimulated chemists to design new tools for the selective detection of hazardous materials. The utilization of nitroaromatic compounds (NACs) as explosive substances has aroused widespread concern for human health, national security, and the environment in recent years.[1–3] There are several NACs such as nitrobenzene (NB), *p*-nitrotoluene (*p*-NT), *o*-nitrotoluene (*o*-NT), *p*-nitrophenol (*p*-NP), *o*-nitrophenol (*o*-NP), 2,4-dinitrophenol (DNP) and 2,4,6-trinitrophenol (TNP) which are widely used in the industry. TNP is known for its high explosivity rate, thus making it a superior choice for use in destruction over other NACs.[4,5] The larger use and higher solubility in water of TNP has led to severe, catastrophic contamination in water bodies. Therefore, the rapid detection of NACs in aqueous effluents has become a highlighted topic of research.[6–8] The portability and sensitivity of optical approaches involving fluorescent probes have garnered significant interest despite many other techniques being well-known in the literature.[9–13] The luminescent properties of the probes mainly depend on the structure, the electron-rich nature of the aromatic ligand, and the metal center.[14,15] The sensing ability by quenching the fluorescence is generally realized by transferring the photoexcited electrons from an electron-rich probe to the electron-deficient analytes.[16]

The compounds of non-transition metals, such as $Zn^{2+}$and Cd^{2+}, exhibit prominent luminescence over other transition metals, thus making them useful in OLED devices and various emitting appliances. Armaroli *et al.* has well-documented the luminescent properties of zinc, cadmium, and other metal compounds in their recent review.[17] A slight modification to ligand topology in Zn(II) compounds has led to improved stability, enhancement in emission intensity, and changes in emission energies. The mononuclear Zn(II) compounds of varying denticity N-donor ligands have been discovered to exhibit photoluminescent properties.[18,19] Several Zn(II) compounds with varying ligands have been reported as sensors in detecting hazardous NACs.[20–23] The topologically diverse aliphatic coordination polymers of zinc and cadmium encapsulated with dipyridylamine ligand have shown the "turn-off" luminescence ability in sensing NACs.[24] The ladder-type coordination polymer of cadmium exhibited luminescent properties, which were effectively used in nitroaromatic sensing at very low concentrations.[25] A 3D metal-organic framework of cadmium has been reported in the detection of potential NAC pollutants.[26] The zinc and cadmium compounds of salen-type ligands have been well studied due to their ability to detect nitroaromatics *via* turn-off fluorescence response.[27] The hydrothermally synthesized 2D, 3D topological cadmium cyclohexyldicarboxylate with co-ligand bis(4-pyridylmethyl)piperazine has been sensibly used in nitroaromatic quenching.[28] The

[a] *J. L. Viegas, V. R. Chari, S. N. Dhuri*
School of Chemical Sciences, Goa University, Taleigao Plateau, Goa 403 206, India
E-mail: sndhuri@unigoa.ac.in

[b] *J. L. Viegas*
Carmel College of Arts, Science and Commerce for Women, Nuvem, Goa 403 604, India

Supporting information for this article is available on the WWW under https://doi.org/10.1002/slct.202402704

topological changes in coordinating ligands were experienced, altering the properties of zinc and cadmium compounds. The versatility of multidentate ligands in cadmium carboxylate coordination polymers has influenced overall structure-function properties, resulting in the quenching of nitroaromatics.[29]

The aminopyridine-based multidentate ligands are proven more acceptable in modern coordination chemistry due to their reactivity and stability being controlled by a subtle interplay of electronic and structural properties.[30,31] In recent times, we have been continuously making efforts to tune the topology of multidentate N-donor ligands. This has resulted in a series of first-row transition metal compounds of amino pyridyl-based ligands that showed diverse applications ranging from catalysis to mimicking enzymes.[32–34] We have also demonstrated a significant quenching of NACs using quinoline-based ligands and N-donor ligand-linked cobalt(II) succinate compounds in our recent work.[35,36] In continuation to our efforts in showcasing the ligand topological effects in metal compounds on their various applications, herein, we have synthesized two Zn(II) compounds, $[Zn(L^1)](ClO_4)_2$ (**1**) and $[Zn(L^2)](ClO_4)_2$ (**2**), containing *N*^{1}-(pyridin-2-ylmethyl)-*N*^{2}-(2-((pyridin-2-ylmethyl)amino)ethyl)-ethane-1,2-diamine (L^1) and *N*^{1}-(pyridin-2-ylmethyl)-*N*^{3}-(3-((pyridin-2-ylmethyl)amino)propyl)propane-1,3-diamine (L^2) (Chart 1). The effect of extrapolating the carbon chain of ligand L^2 compared to L^1 on the photoluminescent properties of Zn(II) compounds has been described.

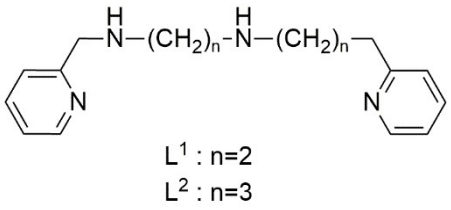

Chart 1: Chemical structures L^1 and L^2 used in this work.

Experimental Section

Material and Methods

Reagents for synthesis and reactivity investigations were bought from commercial sources and did not require further purification. The solvents being used were distilled and dried in a N_2 environment before use. Ligands L^1 and L^2 were prepared following our recent reports.[32,33] Infrared (IR) spectra were recorded on the Shimadzu (IR-Prestige-21) FTIR spectrometer by diluting the compounds in KBr powder in the 4000–400 cm^{-1} region. C, H and N content were obtained using Elementar Variomicro Cube CHNS Analyser. Single crystal X-ray structures of **1** and **2** were determined using Bruker D8 Quest Eco X-ray diffractometer. Intensity data were collected at room temperature (RT) using monochromated (MoKα = 0.7107 Å) radiation. The program suite APEX4 (Version 2021.10-0) was used to integrate the frames, perform absorption correction, and determine the unit cell. The structures were solved with SHELXS, and subsequent refinements were performed with SHELXL.[37] The phase purity of powdered samples was confirmed using powder X-ray diffraction (PXRD) measurements carried out on a Bruker D8 Advance X-ray diffractometer using Cu $k_{\alpha 1}$ (λ = 1.5406 Å) with a nickel filter. The solution state fluorescence spectra were recorded on the Cary Eclipse fluorescence spectrophotometer. ^{1}H NMR spectra were recorded on a Bruker Avance III, 400 MHz, NMR spectrometer using D_2O. The electrospray ionization mass spectra (ESI-MS) of **1** and **2** were recorded using Shimadzu LCMS-2020.

Syntheses of the Zn(II) Compounds

Synthesis of $[Zn(L1)](ClO_4)_2$ (1)

Compound **1** was prepared by slowly adding L^1 (0.38 g, 1.34 mmol) in acetonitrile (5 mL) to the stirring CH_3CN solution of $Zn(ClO_4)_2.6H_2O$ (0.5 g, 1.34 mmol) (2 mL) at room temperature. The mixture was stirred for ~ 5 h. The reaction mixture afforded a colorless crystalline solid upon adding diethyl ether (10 mL). The slow diffusion of diethyl ether into the CH_3CN solution of **1** resulted in white transparent crystals suitable for single crystal x-ray diffraction analysis. The yield of compound **1** was 0.60 g (1.09 mmol) 82 %. *Anal. Calc.* for (**1**) $C_{16}H_{23}Cl_2ZnN_5O_8$ (%): C, 34.96; H, 4.22; N, 12.74. *Found:* C, 34.35; H, 4.10; N, 12.43. IR (KBr, cm^{-1}): 3296 υ(NH); 2980–2883 υ(CH); 1078, 619 υ(ClO_4). ESI-MS: *m/z* = 448.15 (*Calc.* 488.07) for $[Zn(L^1)(ClO_4)]^+$.

Synthesis of [Zn(L2)](ClO4)2 (2)

As mentioned for **1**, a similar methodology was used by reacting L^2 (0.42 g, 1.34 mmol) instead of L^1 to afford colorless crystals of **2**. The yield of **2** was 0.69 g (1.19 mmol), 89 %. *Anal. Calc.* for (**1**) $C_{18}H_{27}Cl_2ZnN_5O_8$ (%): C, 37.42; H, 4.71; N, 12.12. *Found:* C, 37.54; H, 4.37; N, 12.25. IR (KBr, cm^{-1}): 3298 υ(NH); 2950–2872 υ(CH); 1064, 619 υ(ClO_4). ^{1}H NMR (D_2O, ppm): δ 8.47 (d, 2H), δ 7.95 (t, 2H), δ 7.44 (m, 4H), δ 4.27–3.84 (m, 4H), δ 3.19–2.42 (m, 8H), δ 1.81–1.71 (m, 4H). ESI-MS: *m/z* = 476.15 (*Calc.* 476.15) for $[Zn(L^2)(ClO_4)]^+$.

***Caution**! Although we have not experienced accidents, perchlorate salts are potentially explosive in dry states and should be handled in small quantities and with extreme care.*

Photophysical Studies

The photoluminescence properties of compounds **1** and **2** were investigated in the aqueous solution at room temperature. The excitation wavelength was fixed to 370 nm with slit widths (for both excitation and emission) of 10 nm. The experiments were recorded on a Xe flash lamp technology-based Cary Eclipse Fluorescence Spectrophotometer (G9800 A) from Agilent Technologies. In a typical experiment, a 2 mM / 2 mL aqueous solution of **1** or **2** was placed in a 1 cm quartz cuvette, and emission spectra were recorded. For fluorescence sensing titrations of **1** and **2** with the nitroaromatic compounds (NACs), the emission intensities were recorded after the incremental addition of 1 mM NAC solution.

2. Results and Discussion

2.1. Synthesis of Ligands and Compounds 1 and 2

Ligands L^1 and L^2 (Chart 1) were prepared from their diamine precursors, followed by the standard $NaBH_4$ reduction as per our recent reports.[32,33] The Zn(II) compounds, $[Zn(L^1)](ClO_4)_2$ (**1**) and $[Zn(L^2)](ClO_4)_2$ (**2**), were synthesized by reacting $Zn(ClO_4).6H_2O$ with a corresponding CH_3CN solution of the pentadentate ligand (L^1 and L^2) in a 1 : 1 mole ratio (Scheme 1).

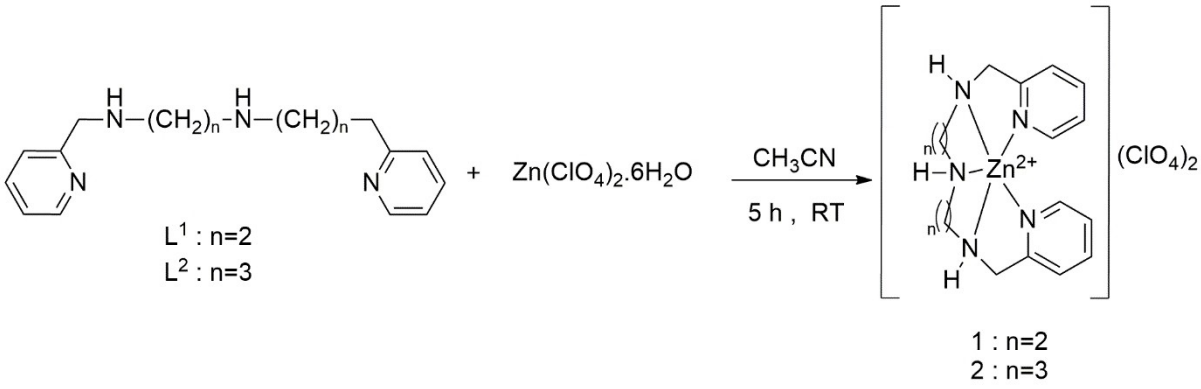

Scheme 1. Synthetic route for preparation of **1** and **2**.

Crystals of compounds **1** and **2**, suitable for single crystal X-ray diffraction analysis, were obtained by slow diffusion of diethylether into the acetonitrile solution in 5 hr. In contrast, in the reported method, **1** was obtained by slow evaporation of aqueous solution after many days.[38] We reinvestigated **1** to compare the influence of increased ligand backbone on the structural parameters with **2** and study its fluorescence properties. A single crystal X-ray diffraction technique was used to determine the spatial structures of **1** and **2**. The summary of crystallographic data and structural refinement results for **1** and **2** are given in Table 1, while the selected bond lengths and angles for both compounds are listed in Table 2. Elemental analysis of **1** and **2** was consistent with the structural composition obtained from single-crystal X-ray diffraction studies.

2.2. Crystal structures of 1 and 2

2.1.1. Crystal Structure of $[Zn(L^1)](ClO_4)_2$ (1)

Single-crystal X-ray diffraction analysis revealed that compound **1** crystallizes in the tetragonal non-centrosymmetric $P4_1$ space group. The asymmetric unit is built from one crystallographically independent $[Zn(L^1)]^{2+}$ cation and two perchlorate anions (Fig. 1, SI Fig. S1). A unique Zn(II) cation is coordinated by the two N atoms of the flexible pyridyl moiety and three N atoms of the symmetric secondary amine backbone, leading to a five-coordinated square pyramidal geometry. The atoms N1, N2, N3, and N5 formed the base of the square pyramid, while N4 occupies the apical position. The pyridyl nitrogen atoms are disposed *syn* to one another. A careful inspection of bond lengths reveals that Zn-N_{py} bond lengths lie in the range 2.125(3)-2.135(3) Å, which are slightly shorter than Zn-N_{amine} bond distances (2.146–2.148(3) Å) due to the hybridization of sp^2 pyridine and sp^3 amine nitrogens.[39] The distortion in coordination geometry around the Zn(II) center can be determined by calculating Addison parameter (τ_5) using the equation $\tau = (\beta - \alpha)/60$, where β and α are the two most prominent coordinate angles.[40–43] The calculated Addison parameter, $\tau_5 = 0.07$, suggested a slight distortion in the square

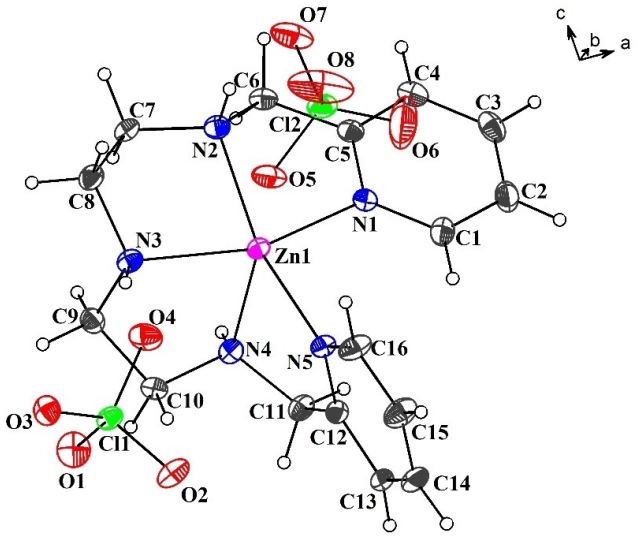

Figure 1. Crystal structure of **1** showing atom labeling scheme. The thermal ellipsoids are drawn at a 30% probability level for all the atoms except for the H atoms, which are shown as spheres of arbitrary radii.

pyramidal geometry of **1**. It is observed that the bond angles of N(1)-Zn(1)-N(3) (157.69°) and N(5)-Zn(1)-N(2) (162.09°) are less than expected 180° in square pyramidal geometry. The perchlorate anions play a significant role in building the supramolecular architecture through its oxygen atoms (O2, O3, O4, and O7), which are involved in non-covalent H-bond interactions (Fig. 2). The predominant intermolecular hydrogen bonds between N–H···O and C–H···O renders additional stability to the crystal structure of **1**. Selected non-covalent H-bonds are summarized in Table 3. The crystal packing of **1** viewed along the *'ab'* plane (SI Fig. S2) illustrates the intercalation of perchlorate counterions with the cation species $[Zn(L^1)]^{2+}$.

Table 1. Crystal data and structure refinement parameters for **1** and **2**.

Empirical formula	$C_{16}H_{23}Cl_2ZnN_5O_8$ (**1**)	$C_{18}H_{27}Cl_2ZnN_5O_8$ (**2**)
Formula weight (g mol^{-1})	549.68	577.74
Temperature (K)	150	150
Wavelength (Å)	0.71073	0.71073
Crystal system	Tetragonal	Monoclinic
Space group	$P4_1$	$P2_1/c$
a (Å)	8.8375(5)	13.6348(7)
b(Å)	8.8375(5)	8.4280(4)
c (Å)	28.034(2)	20.3603(10)
α (°)	90	90
β (°)	90	97.136(2)
γ (°)	90	90
Volume ($Å^3$)	2189.5(3)	2321.6(2)
Z	4	4
Calc. Density (mg/m^3)	1.668	1.653
Absorption coefficient (mm^{-1})	1.420	1.344
F(000)	1128	1192
Diffractometer	Bruker D8 Quest Eco	Bruker D8 Quest Eco
Theta range for data collection (°)	2.305 to 28.277	2.619 to 28.322°
Completeness to theta	100.0	99.8
Index ranges	$-11 \le h \le 11$	$-18 \le h \le 18$
	$-11 \le k \le 11$	$-11 \le k \le 11$
	$-37 \le l \le 37$	$-27 \le l \le 26$
Reflections collected	43081	168996
Independent reflections	5439 [R(int) - = 0.0432]	5767 [R(int) - = 0.0302]
Refinement method	Full-matrix least-squares on F^2	Full-matrix least-squares on F^2
Absorption correction	Semi-empirical from equivalents	Semi-empirical from equivalents
Data/restraints/parameters	5439/1/289	5767/0/288
Goodness-of-fit on F^2	1.052	1.066
Final *R*indices [I > 2sigma(I)]	R1 = 0.0289, wR2 = 0.0665	R1 = 0.0913, wR2 = 0.2346
R indices (all data)	R1 = 0.0367, wR2 = 0.0690	R1 = 0.0949, wR2 = 0.2380
CCDC No.	2309423	2309424

Table 2. Selected bond lengths (Å) and angles (°) for **1** and **2**.

Compound **1**
Zn(1)-N(5) 2.125(3) Zn(1)-N(1) 2.135(3)
Zn(1)-N(4) 2.147(3) Zn(1)-N(3) 2.148(3)
Zn(1)-N(2) 2.146(3)
N(5)-Zn(1)-N(1) 94.94(12) N(5)-Zn(1)-N(2) 162.09(11)
N(1)-Zn(1)-N(2) 78.13(11) N(5)-Zn(1)-N(4) 78.49(11)
N(2)-Zn(1)-N(4) 118.76(12) N(5)-Zn(1)-N(3) 107.24(12)
N(1)-Zn(1)-N(3) 157.69(11) N(2)-Zn(1)-N(3) 81.27(11)
N(4)-Zn(1)-N(3) 82.63(11) N(1)-Zn(1)-N(4) 99.85(11)
Compound **2**
Zn(1)-N(3) 2.043(3) Zn(1)-N(1) 2.090(5)
Zn(1)-N(4) 2.118(5) Zn(1)-N(5) 2.165(5)
Zn(1)-N(2) 2.174(5)
N(3)-Zn(1)-N(1) 123.8(3) N(3)-Zn(1)-N(4) 102.0(3)
N(1)-Zn(1)-N(4) 134.0(18) N(3)-Zn(1)-N(5) 100.2(3)
N(1)-Zn(1)-N(5) 95.3(2) N(4)-Zn(1)-N(5) 79.1(2)
N(3)-Zn(1)-N(2) 93.6(3) N(1)-Zn(1)-N(2) 77.8(19)
N(4)-Zn(1)-N(2) 96.8(2) N(5)-Zn(1)-N(2) 166.1(2)

2.1.2. Crystal Structure of $[Zn(L^2)](ClO_4)_2$ (2)

The geometrically-related ligand L^2 with a six-carbon secondary amine backbone rather than a four-carbon secondary backbone amine containing L^1 was synthesized and metallated with zinc perchlorate to afford compound **2**. The topology of the ligands L^1 and L^2 has led to interesting structural changes in $[Zn(L^2)](ClO_4)_2$ **1** and $[Zn(L^2)](ClO_4)_2$ **2**. The single crystal X-ray diffraction study of **2** reveals that it crystallizes in a centrosymmetric monoclinic space group $P2_1/c$. The asymmetric unit consists of a centrally located Zn(II) cation, a pentadentated L^2 ligand, and two crystallographically independent perchlorate anions (Fig. 3, SI Fig. S3). The carbon atoms C7-C12 and N3 are disordered over two positions, which are modeled with occupancies of 0.64 and 0.36 (SI Fig. S4). The Zn–N bond lengths are similar in both positions, which lie in the range 2.043(3)–2.174(5). The pyridine rings are *trans* to one another. It displayed a distorted trigonal bipyramidal arrangement compared to **1**, which is confirmed by Addison parameter $\tau_5 = 0.53$ based on two relevant angles N(5)-Zn(1)-N(2) (166.1 °) and N(1)-Zn(1)-N(4) (134.0 °), β and α respectively. Thus, a more significant distortion was observed from square pyramidal to trigonal bipyramidal in compound **2**. The non-coordinated perchlorate ions form weak non-covalent N–H···O interactions (Table 3, SI Fig. S5). The crystal packing of compound **2** depicts the arrangement of the cations and anions into alternating layers along the *a*-axis (SI Fig. S6).

2.2. IR spectra, PXRD, ESI-MS, and ^{1}H NMR

The IR spectra of compounds **1** and **2** (SI Fig. S7) exhibit moderately strong peaks in the 3290–3298 cm^{-1} range, assigned to the N–H stretching vibrations arising from L^1 and L^2, respectively. In addition, a sharp peak due to pyridyl C=N stretching is observed between 1605–1608 cm^{-1}. A robust, intense absorption band in the range of 1063–1079 cm^{-1} is assigned to the stretching frequencies of $[ClO_4]^-$ ions. The involvement of hydrogen bonding of perchlorate ions in the

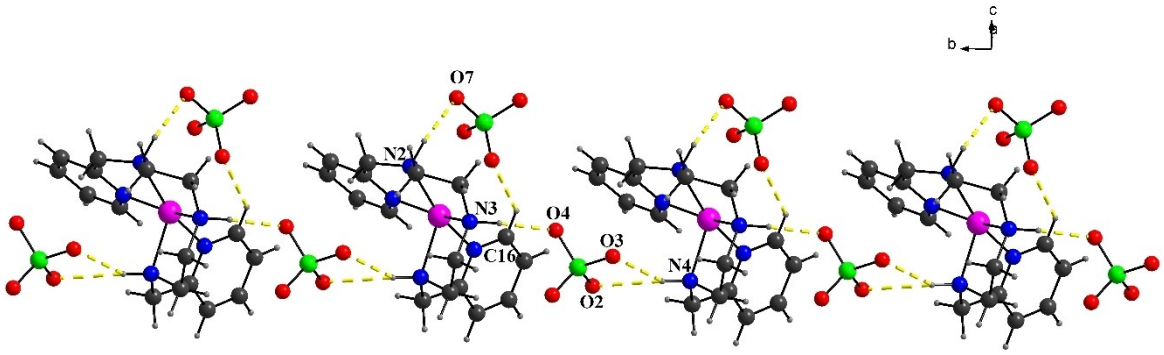

Figure 2. Hydrogen bonding interactions in **1** with atom labeling scheme of atoms involved in hydrogen bonding.

Table 3. Hydrogen bonding parameters for **1** and **2**.

D-H···A	D-H/Å	H···A/Å	D···A/Å	D-H···A/°	Symmetry code
1					
N2-H2···O7	0.980	2.115	3.055	160.11	x, y, z
N3-H3···O4	0.980	2.019	2.978	165.45	x, y, z
N4-H4···O2	0.980	2.428	3.233	139.15	x, y+1, z
N4-H4···O3	0.980	2.197	3.101	152.87	x, y+1, z
C16-H16···O5	0.930	2.432	3.088	127.54	x, y, z
2					
N3-H3A···O5	0.980(0)	2.087(0)	3.059(0)	171.04(0)	x, y, z
N5-H5B ···O4	0.980(0)	2.228(1)	3.179(2)	163.25(0)	x, y, z

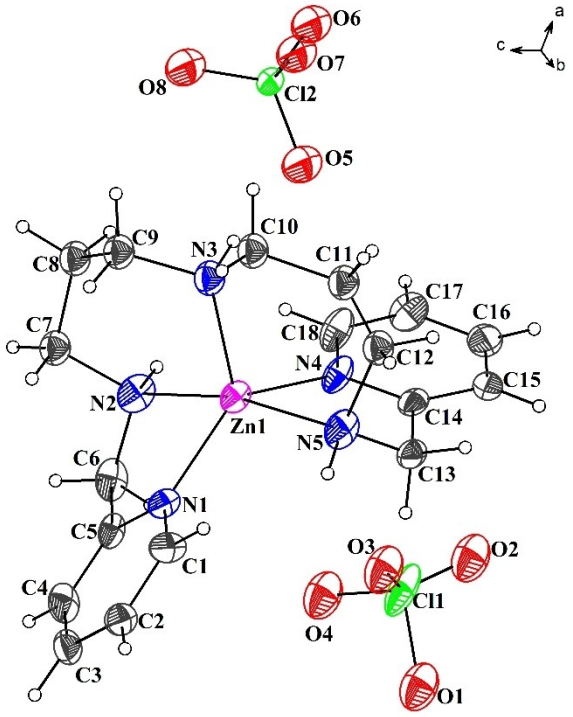

Figure 3. Crystal structure of **2** showing atom labeling scheme. The thermal ellipsoids are drawn at a 30% probability level for all the atoms except for the H atoms, which are shown as spheres of arbitrary radii.

crystal lattices leads to splitting or broadening of the band. The strong band at ~619 cm^{-1} is observed due to the bending mode of vibration for perchlorate ions.[44,45]

Analysis *via* powder X-ray diffraction confirmed the overall purity of synthesized compounds **1** and **2**. The PXRD patterns of **1** and **2** match the findings from single crystal X-ray diffraction data generated with Mercury 4.0 software (Fig. 4).[46]

The stability of compounds **1** and **2** in solution was confirmed by electrospray mass-spectra (ESI-MS), where **1** and **2** exhibits mass peaks at $m/z = 448.15$ (*Calc.* 488.07) for $[Zn(L^1)(ClO_4)]^+$ and $m/z = 476.15$ (*Calc.* 476.15) for $[Zn(L^2)(ClO_4)]^+$ fragments respectively (SI Fig. S8,S9). Compound **2** was further characterized by ^{1}H NMR spectroscopy (SI Fig. S10).

2.3. Photophysical properties of 1 and 2

Compound **1** displayed a prominent peak at 470 nm, whereas compound **2** showed a strong peak at 460 nm when excited with a 370 nm wavelength. These emissions are due to the intra-ligand transitions of $\pi^* \rightarrow n$ and $\pi \rightarrow \pi^*$ of the ligands L^1 and L^2.[47] Once the distinct emission bands were identified, we decided to investigate the sensing properties of **1** and **2** with nitroaromatic compounds (NACs). The electron-deficient NACs employed in this study were nitrobenzene (NB), *o*-nitrotoluene (*o*-NT), *p*-nitrotoluene (*p*-NT), *o*-nitrophenol (*o*-NP), *p*-nitrophenol (*p*-NP), 2,4-dinitrophenol (DNP) and 2,4,6- trinitrophenol

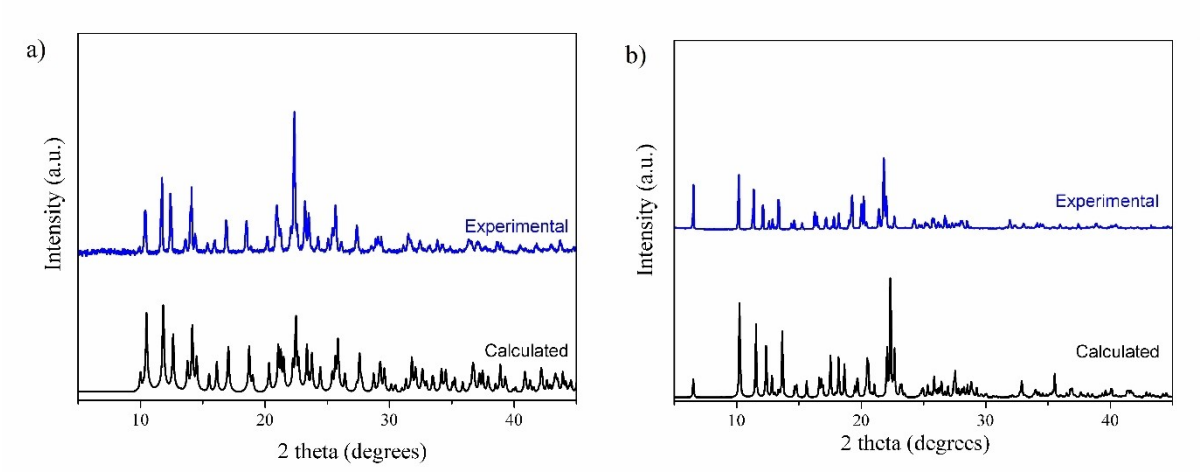

Figure 4. Powder X-ray diffraction patterns for compounds **1 (a)** and **2 (b).**

(TNP). On addition of aqueous solutions of NACS to the aqueous solution of **1**, quenching was observed at 470 nm. The emission titration of **1** with TNP is displayed in Figure 5, and the titration spectra of **1** with remaining NACs are presented in SI Fig. S11-S16. The fluorescence measurements were carried out repeatedly, a minimum of three times, to ensure consistent results. In every instance, adding NACs gradually led to a significant reduction in the initial fluorescence intensity of **1**. The quenching efficiency (η) was determined using the equation provided below;

$$[(I_0 - I)/I_0]x100\% \quad \text{(i)}$$

where I_0 and I are the fluorescence intensities before and after adding the respective NACs. Among all the NACs tested, we observed that in the case of TNP, the initial emission intensity was quenched by almost 98% (η) on adding 200 μL TNP to the solution of **1**. Similarly, on adding DNP (200 μL) to **1**, there was about 96% quenching of the emission band at 470 nm. For other NACs, the emission intensity dropped to 46% for *o*-NP and 42% for *p*-NP. A very sluggish decay of the emission band of **1** was observed with NB, *o*-NT, and *p*-NT, leading to about 31–36% quenching.

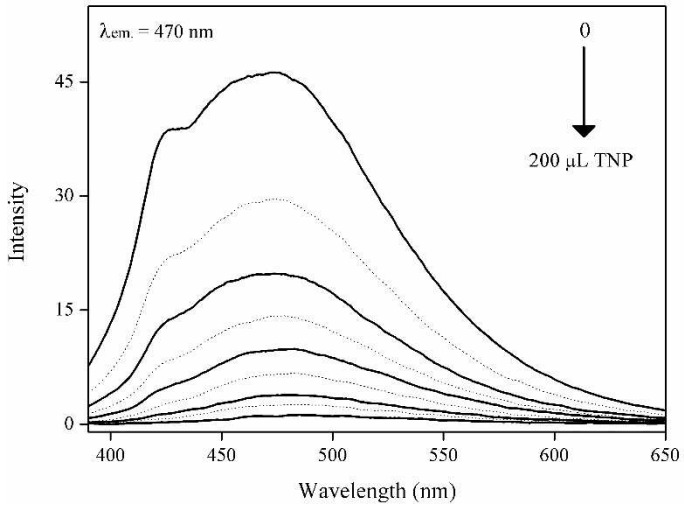

Figure 5. The decay of fluorescence emission peak of **1** ($\lambda_{ex.}$=370 nm) upon gradual addition of 1 mM of trinitrophenol (TNP).

Thus, the quenching efficiency followed the order: NB < *o*-NT < *p*-NT < *p*-NP < *o*-NP < DNP < TNP for all tested NACs. The sensing ability of **1** towards the different NACs is plotted in terms of their quenching efficiencies (%), as depicted in Figure 6. Compound **1** showed remarkably higher quenching efficiency towards dinitro and tri-nitrophenols over other NACs. The results unambiguously indicated that **1** could be selectively used as a chemical sensing reagent in detecting TNP and DNP from an aqueous mixture of other NACs.

Furthermore, the Stern-Volmer (S–V) quenching constant (K_{sv}) was determined by analyzing the normalized fluorescence emission intensity (I_0/I) at different quencher concentrations [Q] using the equation; $I_0/I = 1 + K_{sv}$ [Q] where I_0 and I are the emission intensities of **1**, before and after addition of NACs respectively, K_{sv} is the quenching constant (M^{-1}) and [Q] is the molar concentration of NACs. The S–V plots of **1** with the NACs are shown in Figure 7 (SI Fig. S18). The plots illustrate that the S–V curves for TNP and DNP followed a straight line at low concentrations but diverged into a curved shape at higher concentrations. The quenching constant (K_{sv}) of **1** was obtained from the slope of the equation line, $I_0/I = 1 + K_{sv}$ [Q]. The quenching constants for TNP and DNP are more significant than the other NACs used in this work (SI Table S1). This signified the exclusive quenching ability of TNP and DNP towards luminescent **1** in water, amongst other NACs.[6,13]

Similarly, the fluorescent titrations were performed with compound **2** in water. Compound **2** exhibited emission at 460 nm upon excitation at 370 nm. On screening **2** with the NACs mentioned earlier, the best quenching results were obtained for DNP and TNP. The titration of **2** with TNP is shown in Figure 8, while the titration with DNP is provided in the Supporting Information (SI Fig. S17). On calculating the quenching efficiencies (% η), the initial emission intensity of **2** was

Figure 6. Representation of the quenching efficiency of **1** towards different NACs.

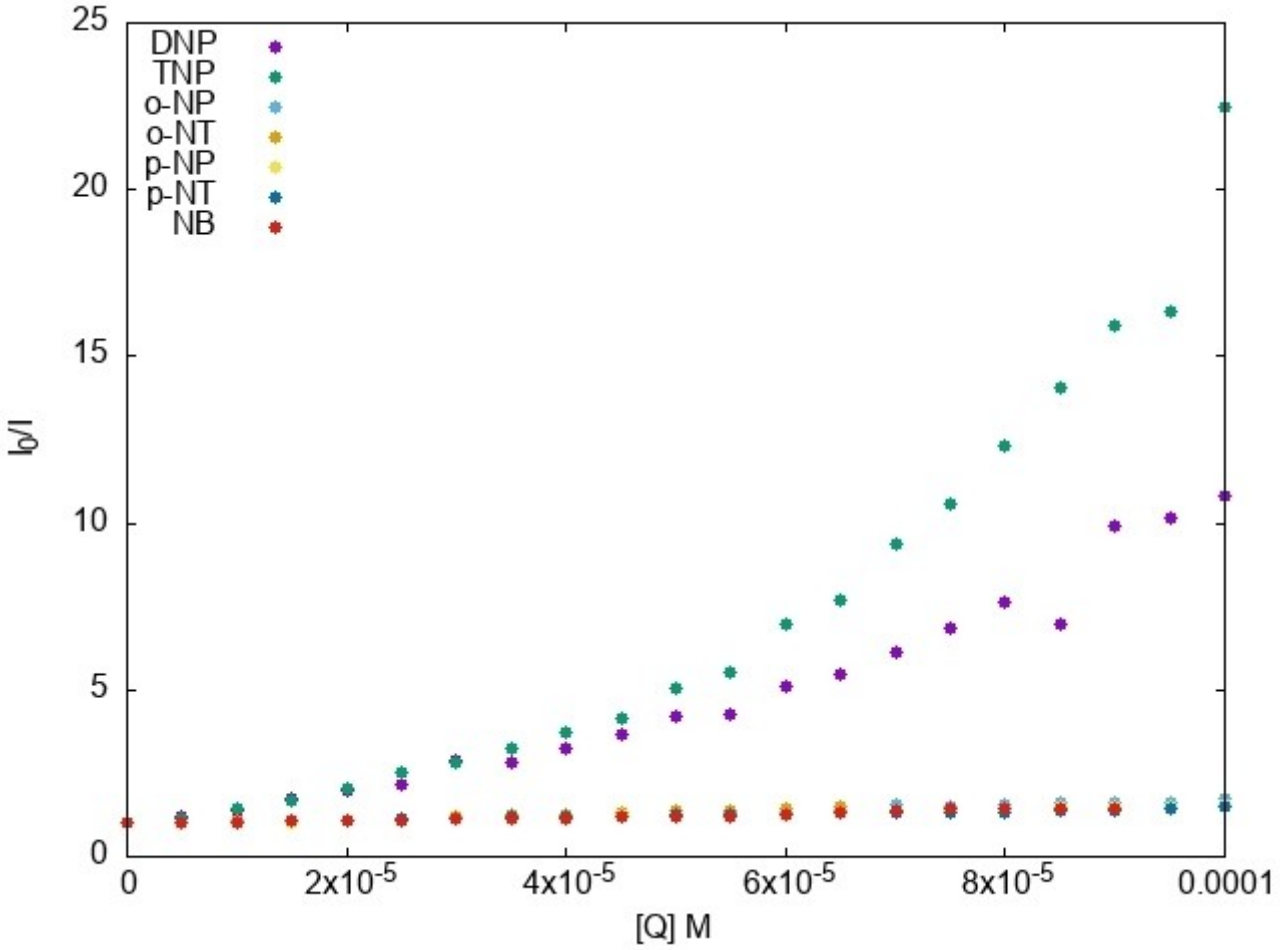

Figure 7. Stern-Volmer plots for NACs added to **1** in water.

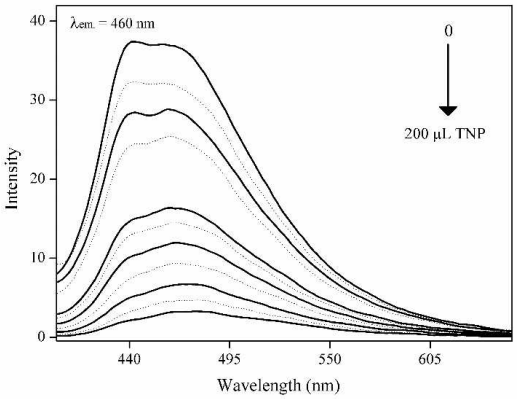

Figure 8. The reduction of fluorescence emission of **2** ($\lambda_{ex.}$ = 370 nm) upon gradually adding 1 mM of 2,4,6- trinitrophenol (TNP).

quenched by 87% for 200 µL of DNP while 92% after 200 µL of TNP. Compound **1** exhibits K_{sv} values almost twice as high as **2** for TNP and DNP.

To gain more insight into the quenching mechanism exhibited by compounds **1** and **2**, the Stern-Volmer plots were investigated. It was observed that the TNP and DNP showed a second-order polynomial fit for the S–V plot, whereas other NACs showed a linear response. While both **1** and **2** exhibit a non-linear response to the addition of TNP and DNP, a linear relationship is observed in the S–V plot at lower concentrations of the NACs (SI Fig. S19 and S20). Second-order polynomial fitting for an NAC indicates the presence of static and dynamic quenching mechanisms in the system.[48]

The degree of spectral overlap between the absorption band of the NACs and the emission band of the compounds determines the likelihood of the resonance energy transfer (RET) mechanism for increased quenching. The existence of spectral overlap in the absorption spectra of TNP and DNP with the emission spectra of the compound indicates the RET mechanism for enhanced quenching. In contrast, the remaining NACs do not exhibit such overlap (SI, Fig S21). As seen (SI, Fig. S21a), in contrast to the other NACs, which exhibit little to no spectral overlap, the absorption spectra of TNP and DNP exhibit significant overlap with the 470 nm emission band of **1**. Consequently, TNP and DNP exhibit higher quenching reactions in comparison to the remaining NACs. Similarly, on verifying the spectral overlap concerning **2** (SI, Fig. S21b), there was considerable overlap between the emission band of **2** with TNP and DNP, thereby suggesting the practical quenching ability of **2** towards TNP and DNP. However, it was observed that the adequate overlap was more in the case of **1** as compared to **2**. These observations suggest that **1** demonstrates superior selectivity towards TNP and DNP sensing over **2**, which has a more extended carbon chain backbone. Thus, the topology of ligand L^1 and the structure of compound **1** dominate the reactivity with nitroaromatic compounds.

3. Conclusions

This study investigated structural, spectroscopic and photophysical properties two Zn(II) compounds, $[Zn(L^1)](ClO_4)_2$ (**1**) and $[Zn(L^2)](ClO_4)_2$ (**2**). Compound **1** was revisited to understand the influence of ligand structure on the electronic property of **1** and compare it with a new compound 2 stabilized by L^2. The distinct and noticeable influence of the difference in ligand topology was seen in the reactivity patterns of **1** and **2** with NAC substrates. Compound **1** demonstrates superior selectivity towards sensing of TNP and DNP over compound **2**, which has a longer carbon chain backbone. This has been demonstrated by the overlap of the absorption band with the emission band, and the overlap is more prominent in compound **1**.

Supporting Information Summary

The supplementary material contains additional figures (Figure S1–S21) and table (Table S1). The crystal cif structure data and check if of compounds **1** and **2** are also given in supplementary material. Crystal structure Deposition Number(s): CCDC 2309423 (for **1**) and 2309424 (for **2**), contain(s) the supplementary crystallographic data for this paper. These data are provided free of charge by the joint Cambridge Crystallographic Data Centre and Fachinformationszentrum Karlsruhe Access Structures service "http://www.ccdc.cam.ac.uk/structures".

Acknowledgements

SND acknowledged the Council of Scientific and Industrial Research, New Delhi (No. 01(2923)/18/EMR-II) and Goa State Research Foundation, Goa (GSRF/Schemes/MajorGR /13/2023/187/ii) for research support. JLV thanks the government of Goa for the Study Leave. Authors greatly acknowledge the support from the Department of Science and Technology, New Delhi (SR/FST/CSII-034/2014(C), and SR/PURSE/2023/198 to the School of Chemical Sciences, Goa University. The authors also thank the University Grants Commission, New Delhi, for supporting the School of Chemical Sciences, Goa University, under the UGC-SAP program (F.504/14/DSA-I/2015).

Conflict of Interests

The authors declare no conflict of interest.

Data Availability Statement

The data that support the findings of this study are available from the corresponding author upon reasonable request.

Keywords: Zinc · Pentadendate · Nitrogen donor · Crystal structure · Nitroaromatics

[1] J. S. Caygill, F. Davis, S. P. J. Higson, *Talanta* **2012**, *88*, 14–29.
[2] E. A. Naumenko, B. Ahlemeyer, E. Baumgart-vogt, *Environ. Toxicol.* **2017**, *3*, 989–1006.
[3] T. M. Mallon, J. M. Ortiz, W. H. Candler, G. Rogers, R. Hillburn, *Mil. Med.* **2014**, *179*, 1374–1383.
[4] G. He, H. Peng, T. Liu, M. Yang, Y. Zhang, Y. Fang, *J. Mater. Chem.* **2009**, *19*, 7347–7353.
[5] Y. Peng, A.-J. Zhang, M. Dong, Y.-W. Wang, *Chem. Commun.* **2011**, *47*, 4505–4507.
[6] Y. Meng, N. Zhang, J. Li, Y. Xu, Q. Yang, Y. Yuan, X. Zhang, J. Wub, L. Zhao, *Spectrochim. Acta Part A* **2022**, *266*, 120419.
[7] S. S. Nagarkar, A. V Desai, P. Samanta, S. K. Ghosh, *Dalton Trans.* **2015**, *44*, 15175–15180.
[8] Y. Deng, N. Chen, Q. Li, X. Wu, X. Huang, Z. Lin, Y. Zhao, *Cryst. Growth Des.* **2017**, *17*, 3170–3177.
[9] D. S. Moore, *Rev. Sci. Instrum.* **2004**, *75*, 2499–2511.
[10] S. Wang, H. Chen, *J. Chromatogr. A.* **2002**, *979*, 439–446.
[11] H. Ebrahimzadeh, Y. Yamini, F. Kamarei, *Talanta* **2009**, *79*, 1472–1477.
[12] R. Wilson, C. Clavering, A. Hutchinson, *Anal. Chem.* **2003**, *75*, 4244–4249.
[13] A. Jana, J. Mandal, S. S. Mondal, R. Patra, A. Bhunia, *Inorg. Chim. Acta.* **2023**, *549*, 121409.
[14] A. Gusev, V. Shul'gin, E. Braga, E. Zamnius, M. Kryukova, W. Linert, *Dyes Pigm.* **2020**, *183*, 108626.
[15] X. Song, Y. Peng, G. Cheng, X. Wang, P. Liu, W. Xu, *Inorg. Chim. Acta.* **2015**, *427*, 13–21.
[16] S. Shanmugaraju, P. S. Mukherjee, *Chem. Eur. J.* **2015**, *21*, 6656–6666.
[17] A. Barbieri, G. Accorsi, N. Armaroli, *Chem. Commun.* **2008**, *19*, 2185–2193.
[18] M. Shyamal, A. Panja, A. Sah, *Polyhedron* **2014**, *69*, 141–148.
[19] V. Amani, *J. Mol. Struct.* **2018**, *1155*, 477–483.
[20] Y. Ma, G. Xu, F. Wei, Y. Cen, Y. Song, M. Shi, X. Xu, M. Sohail, Q. Hu, *New J. Chem.* **2018**, *42*, 5162–5167.
[21] T. Chatterjee, E. Hossain, S. Khan, S. Roy, S. M. Wabaidur, M. A. Islam, S. M. Alam, M. H. Mir, *J. Mol. Struct.* **2023**, *1271*, 134011.
[22] A. S. Burlov, V. G. Vlasenko, Y. V Koshchienko, N. I. Makarova, A. A. Zubenko, Y. D. Drobin, G. S. Borodkin, A. V Metelitsa, Y. V Zubavichus, D. A. Garnovskii, *Polyhedron* **2018**, *144*, 249–258.
[23] D. Mukherjee, K. Sarkar, S. Reja, M. Bakibillah, S. Guha, N. K. Mandal, J. P. Naskar, R. K. Das, *J. Fluoresc.* **2023**.
[24] Z. I. Contejean, R. L. LaDuca, *J. Solid State Chem.* **2018**, *266*, 44–53.
[25] B. Dutta, S. Paul, S. Halder, *Heliyon* **2023**, *9*, e13504.
[26] J.-L. Du, X. Lu, T.-L. Shen, C.-P. Li, Y.-J. Mu, L.-J. Li, *Mater. Lett.* **2015**, *158*, 225–228.
[27] S. Roy, I. Mondal, K. Harms, S. Chattopadhyay, *Polyhedron* **2019**, *159*, 265–274.
[28] A. R. LaDuca, R. L. LaDuca, *CrystEngComm* **2018**, *20*, 5677–5687.
[29] X. -Z. Guo, S. -S. Chen, W. -D. Li, S. -S. Han, F. Deng, R. Qiao, Y. Zhao, *ACS Omega* **2019**, *4*, 11540–11553.
[30] A. G. Blackman, *Polyhedron* **2019**, *161*, 1–33.
[31] W. K. C. Lo, C. J. McAdam, A. G. Blackman, J. D. Crowley, D. A. McMorran, *Inorg. Chim. Acta.* **2015**, *426*, 183–194.
[32] D. D. Narulkar, A. K. Srivastava, R. J. Butcher, K. M. Ansy, S. N. Dhuri, *Inorg. Chim. Acta.* **2017**, *467*, 405–414.
[33] J. L. Viegas, S. N. Dhuri, *J. Mol. Struct.* **2023**, *1288*, 135719.
[34] D. D. Narulkar, K. Devulapally, A. K. U. S. N. Dhuri, *Sustain. Energy Fuels* **2020**, *4*, 2656–2660.
[35] S. S. Harmalkar, A. V. Naik, M. K. Nilajakar, S. N. Dhuri, *ChemistrySelect* **2020**, *5*, 8447–8454.
[36] L. R. D'souza, N. N. Harmalkar, S. S. Harmalkar, S. B. Tayade, S. N. Dhuri, *ACS Omega* **2022**, *7*, 5698–5712.
[37] G. M. Sheldrick, *Acta Crystallogr. Sect. C* **2015**, *71*, 3–8.
[38] J. Lin, N. Wang, X. Chen, X. Yang, L. Hong, Z. Ruan, H. Ye, Y. Chen, X. Liang, *Sustain. Energy Fuels* **2022**, *6*, 1312–1318.
[39] W. P. Sohtun, S. Muthuramalingam, M. Velusamy, R. Mayilmurugan, *Inorg. Chem. Commun.* **2019**, *110*, 107608.
[40] A. W. Addison, T. N. Rao, J. Reedijk, J. van Rijn, G. C. Verschoor, *Dalton Trans.* **1984**, *7*, 1349–1356.
[41] L. Yang, D. R. Powell, R. P. Houser, *Dalton Trans.* **2007**, *9*, 955–964.
[42] A. G. Blackman, E. B. Schenk, R. E. Jelley, E. H. Krenske, L. R. Gahan, *Dalton Trans.* **2020**, *49*, 14798–14806.
[43] S. Alvarez, M. Llunell, *Dalton Trans.* **2000**, *19*, 3288–3303.
[44] A. Panja, *Dalton Trans.* **2014**, *43*, 7760–7770.
[45] S. S. Harmalkar, R. J. Butcher, V. V. Gobre, S. K. Gaonkar, L. R. D'Souza, M. Sankaralingam, I. Furtado, S. N. Dhuri, *Inorg. Chim. Acta.* **2019**, *498*, 119020.
[46] C. F. MacRae, I. Sovago, S. J. Cottrell, P. T. A. Galek, P. McCabe, E. Pidcock, M. Platings, G. P. Shields, J. S. Stevens, M. Towler, P. A. Wood, *J. Appl. Crystallogr.* **2020**, *53*, 226–235.
[47] D. Das, B. G. Chand, J. Dinda, C. Sinha, *Polyhedron* **2007**, *26*, 555–562.
[48] A. S. Tanwar, R. Parui, R. Garai, M. A. Chanu, P. K. Iyer, *ACS Meas. Sci. Au.* **2022**, *2*, 23–30.

Manuscript received: June 5, 2024